Aalborg Universitet

AALBORG UNIVERSITY
DENMARK

On the Potential of Interference Rejection Combining in B4G Networks

Tavares, Fernando Menezes Leitão; Berardinelli, Gilberto; Mahmood, Nurul Huda; Sørensen, Troels Bundgaard; Mogensen, Preben

Link to publication from Aalborg University

On the Potential of Interference Rejection Combining in B4G Networks

Fernando M. L. Tavares, Gilberto Berardinelli, Nurul H. Mahmood, Troels B. Sørensen, and Preben Mogensen

Department of Electronic Systems, Aalborg University

Niels Jernes Vej 12, 9220 Aalborg Øst, Denmark

ft@es.aau.dk

Abstract—**Beyond 4th Generation (B4G) local area networks will be characterized by the dense uncoordinated deployment of small cells. This paper shows that inter-cell interference, which is a main limiting factor in such networks, can be effectively contained using Interference Rejection Combining (IRC) receivers. By simulation we investigate two significantly different interference scenarios with dense small cell deployment. The results show that IRC brings considerable improvement in outage as well as in peak and median throughputs in both scenarios, and thus has a big potential as a capacity and coverage enhancing technique for B4G. The IRC gain mechanism depends strongly on the interference scenario and to some extent on the use of frequency reuse. These results are achieved with no coordination among cells and suggests that Multiple Input Multiple Output (MIMO) rank adaptation and IRC can be performed independently.**

I. Introduction

In the last decades, several generations of Radio Access Networks (RANs) have been designed to cope with the growing demand for wireless services. A new disruptive system has emerged approximately every 10 years to alleviate backward compatibility problems and to take advantage of the evolution of the technology components. Considering that the specifications of the Long Term Evolution - Advanced (LTE-A) radio standard were submitted in 2010, a novel Beyond 4th Generation (B4G) RAN is then expected to emerge in the market around 2020 [1].

This new RAN should be designed to support the massive deployment of small cells, since this type of deployment is foreseen as a solution for meeting the future capacity expansion requirements [1]. As deployments become denser, their uncoordinated nature will inevitably aggravate the inter-cell interference problem, causing considerable impact on the network performance. The allocation of orthogonal spectrum resources to cells that strongly interfere with each other is often considered as the solution for this problem [2], [3].

With the evolution of electronic hardware and Multiple Input Multiple Output (MIMO) techniques, inter-cell interference suppression techniques, whose application was previously limited by their large computational burden, may now be cost-effectively implemented in receivers. It is reasonable to believe that this kind of receivers can offer high performance gains in interference limited scenarios, but, to the best of our knowledge, all the system level performance evaluation studies on the topic focus on macro cell and heterogeneous LTE and LTE-A network scenarios [4]–[7].

Different baseband processing techniques may be used to suppress the inter-cell interference. For instance, Successive Interference Cancellation (SIC) and Parallel Interference Cancellation (PIC) techniques decode both the desired and the interfering signal to cancel their mutual interference contribution [8]. Conversely, Interference Rejection Combining (IRC) is a linear combining technique that relies on multiple receive antennas and the estimate of the interfering channels to project the received signals on a subspace in which the Mean Square Error (MSE) is minimized [9]. IRC is attractive given its simplicity and maturity, and it represents a straightforward add-on to the known Minimum Mean Square Error (MMSE) detector, which is now considered the baseline detector in LTE networks [10].

In this paper, we present the first system level downlink performance evaluation of inter-cell interference suppression for different local area small cell B4G scenarios. Specifically, we consider scenarios with dense small cell deployment and two modes of operation: one with closed subscriber mode of relevance for office buildings (or private apartments) and one with open subscriber mode of relevance for public hot spots. We use a signal model that includes spatial multiplexing precoding with multiple data layers (both for the desired and the interfering signals) to verify their effects on the interference rejection capabilities of IRC and contrast it with the use of different frequency reuse schemes. Our ultimate goal is to address the effective potential of this detector on the performance of B4G networks, providing information that will help guide the design of this new RAN.

The paper is organized as follows. We first describe the signal model used in the simulations in Section II and the details related to the simulation setup in Section III; we present and analyse the simulation results in Section IV; finally, we draw our conclusions in Section V.

II. Signal Model

In this section, we present the analytical signal model of the detectors that are used in our system evaluation.

We assume that the generic i-th network node is equipped with N_{tx} transmit antennas and N_{rx} receive antennas, and can transmit $1 \leq N_{streams_i} \leq min(N_{rx}, N_{tx})$ data streams. The number of transmitted streams is also often referred as transmission *rank*. For simplicity, we present the system model

for a generic Orthogonal Frequency Division Multiplexing (OFDM) frequency subcarrier.

Let us denote with $\mathbf{s}_i$ the $N_{streams_i} \times 1$ data column vector of the i-th node. The vector $\mathbf{s}_i$ is mapped over the N_{tx} antennas by the $N_{tx} \times N_{streams_i}$ precoding matrix $\mathbf{C}_i$. Let us assume that the subscript D denotes the desired signal at the receiver side, and the subscript I_q the q-th interfering signal. After transmission over the fading channel, the $N_{rx} \times 1$ frequency domain received column vector at a particular receiver can then be expressed as

$$\mathbf{r} = \tilde{\mathbf{H}}_D \mathbf{s}_D + \tilde{\mathbf{H}}_I \mathbf{s}_I + \mathbf{n} \tag{1}$$

where

- $\mathbf{n}$ is the $N_{rx} \times 1$ Additive White Gaussian Noise (AWGN) contribution vector with power σ_0^2;
- $\tilde{\mathbf{H}}_D$ and $\tilde{\mathbf{H}}_{I_q}$ are the equivalent channel matrices which include the precoding matrices, i.e. $\tilde{\mathbf{H}}_D = \mathbf{H}_D \mathbf{C}_D$ and $\tilde{\mathbf{H}}_{I_q} = \mathbf{H}_{I_q} \mathbf{C}_{I_q}$, with $\mathbf{H}_D$ and $\mathbf{H}_{I_q}$ being the $N_{rx} \times N_{tx}$ fading channel matrices;
- $\mathbf{s}_I$ and $\tilde{\mathbf{H}}_I$ represent the concatenation of the N_I received interfering signals and the concatenation of their equivalent N_I channels, respectively, i.e.

$$\mathbf{s}_I = [\mathbf{s}_{I_1}^T \ldots \mathbf{s}_{I_q}^T \ldots \mathbf{s}_{I_{N_I}}^T]^T \tag{2}$$

$$\tilde{\mathbf{H}}_I = [\tilde{\mathbf{H}}_{I_1} \ldots \tilde{\mathbf{H}}_{I_q} \ldots \tilde{\mathbf{H}}_{I_{N_I}}] \tag{3}$$

where $(\cdot)^T$ denotes the transpose operator.

Let us also define the generic MMSE combining matrix [11]:

$$\mathbf{W} = (\hat{\mathbf{H}}_D \hat{\mathbf{H}}_D^H + \mathbf{R}_n)^{-1} \hat{\mathbf{H}}_D \tag{4}$$

where $(\cdot)^H$ is the hermitian operator and $\hat{\mathbf{H}}_D$ represents the estimated equivalent channel matrix of the desired signal.

The desired $\hat{\mathbf{s}}_D$ is then estimated by using the combining matrix $\mathbf{W}$:

$$\hat{\mathbf{s}}_D = \mathbf{W}^H \mathbf{r} \tag{5}$$

The following detectors can be specified according to the nature of the matrix $\mathbf{R}_n$:

- *MMSE - Interference Rejection Combining (MMSE-IRC):*

$$\mathbf{R}_n = E\{\hat{\mathbf{H}}_I \hat{\mathbf{H}}_I^H\} + \sigma_0^2 \mathbf{I}_{\mathbf{N_{rx}}} \tag{6}$$

where $\mathbf{I}_{\mathbf{N_{rx}}}$ denotes the $N_{rx} \times N_{rx}$ identity matrix.

- *MMSE - Maximal Ratio Combining (MMSE-MRC):*

$$\mathbf{R}_n = \mathrm{diag}([m_1 \cdots m_{N_{rx}}]) \tag{7}$$

where

$$m_z = E\left\{ \sum_{q=1}^{N_I} \sum_{k=1}^{N_{streams_q}} \left| \hat{\mathbf{H}}_{I_{q(z,k)}} \right|^2 \right\} + \sigma_0^2 \tag{8}$$

with $\hat{\mathbf{H}}_{I_{q(z,k)}}$ corresponding to the element in the z-th row and the k-th column of $\hat{\mathbf{H}}_{I_q}$.

While in the MMSE-MRC detector the matrix $\mathbf{R}_n$ can be computed by estimating the total interference plus noise power

Physical Layer Model [1]		
Spectrum Allocation	200 MHz at 3.5 GHz	
Frame Duration	0.25 ms	
Access Scheme	Downlink OFDMA 3000 subcarrriers 60 kHz each 15 subcarriers per PRB	
Transmission Power	20 dBm	
Receiver Noise Figure	9 dB	
MIMO Scheme	Closed-loop SU-MIMO with dynamic rank and precoder adaptation	
Spectral Efficiency Model		
Maximum Spectral Efficiency	6 bits/s/Hz	64 QAM (1/1)
Error Vector Magnitude	5%	$\mathrm{SINR}_{max} \approx 26$dB

at each receive antenna, $\mathbf{R}_n$ in the MMSE-IRC detector corresponds to the estimated covariance matrix of the interfering signals. Therefore, MMSE-IRC assumes knowledge of each interfering channel at each antenna which may impose strict requirements on the system design since each node would need to discriminate the reference sequences sent by multiple interferers. We assume here that such a system design is possible, and consider it to be a topic for future work.

III. SIMULATION SETUP

As mentioned in the introduction, the usage of IRC detectors is foreseen as particularly beneficial in scenarios characterized by a dense uncoordinated deployment of small cells. This paper aims at addressing such potential with an extensive system level evaluation. In this section, we describe in details the physical layer assumptions, scenarios and simulation setup used in our simulation campaign.

A. Physical Layer Assumptions

We assume ideal channel estimation of both desired and interfering signals based on the aforementioned reference sequences. Rank and precoding adaptation feedback with no errors and one frame delay is assumed. The precoding matrices used are those defined in [12] for downlink closed-loop single-user MIMO in LTE, and are applied per Physical Resource Block (PRB) in frequency domain for the assumed OFDM based system [1].

We calculate the Signal-to-Interference-plus-Noise Ratio (SINR) for the j-th stream as follows [11]:

$$\mathrm{SINR}_j = \frac{\mathbf{W}_{(j)}^H \mathbf{H}_{D_{(j)}} \mathbf{H}_{D_{(j)}}^H \mathbf{W}_{(j)}}{\mathbf{W}_{(j)}^H (\bar{\mathbf{H}}_{D_{(j)}} \bar{\mathbf{H}}_{D_{(j)}}^H + \mathbf{H}_I \mathbf{H}_I^H + \sigma_0^2 \mathbf{I}_{\mathbf{N_{rx}}}) \mathbf{W}_{(j)}} \tag{9}$$

where $\mathbf{A}_{(j)}$ denotes the j-th column of matrix $\mathbf{A}$ and $\bar{\mathbf{A}}_{(j)}$ is the matrix obtained by removing the j-th column from matrix $\mathbf{A}$.
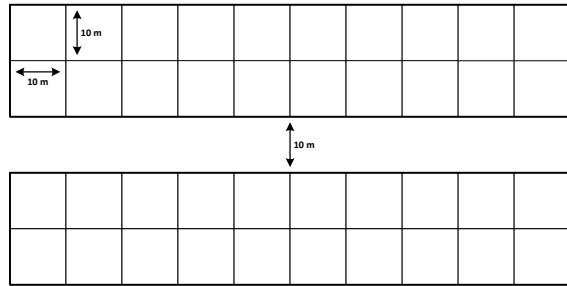
(a) Scenario A - Indoor Office
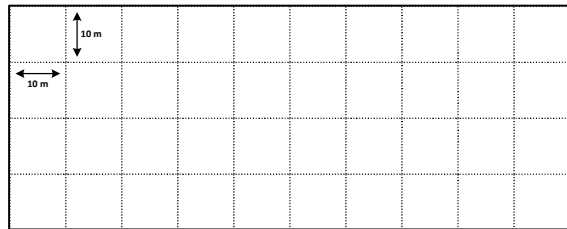
(b) Scenario B - Indoor Hotspot

Fig. 1.   Simulation Scenarios

The SINR values are then adjusted using the following Error Vector Magnitude (EVM) model to account for transceiver implementation imperfections.

$$\text{SINR}_{\text{evm},j} = \frac{\text{SINR}_j \cdot \text{SINR}_{\text{max}}}{\text{SINR}_j + \text{SINR}_{\text{max}}} \qquad (10)$$

Based on the resulting SINR we calculate the corresponding data rate using the Shannon formula, with maximum spectral efficiency limited to 6 bits/s/Hz (uncoded 64QAM modulation). All streams are added, resulting in the total data rate per User Equipment (UE). Table I summarizes these physical layer details.

B. Simulation Scenarios

Two simulation scenarios were selected for this study. Scenario A is an indoor office scenario used for the study of femtocells [13]. This scenario is depicted in Figure 1(a). It consists of two office buildings, each located at one side of a 10 meter wide street. Each building is modelled as two rows of 10 square offices. For simplicity, only one floor was simulated with one UE and one Access Point (AP) randomly placed in each office. Each office may have one active cell under Closed Subscriber Group (CSG) access mode, i.e. the UE can only connect to the AP in the same office and not to any of the neighbour's APs. Large scale propagation effects (pathloss and shadowing) are calculated using the 3GPP Dual Stripe model [13].

Figure 1(b) depicts Scenario B. This scenario simulates an indoor hotspot scenario, similar to an airport check-in hall or a large conference hall, for example. The total area of the hall is divided in square areas and one AP is installed in the center
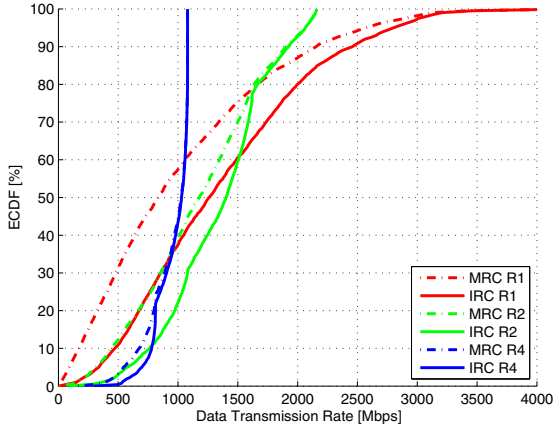
Scenario A - Indoor Office		
Access Mode	Closed Subscriber Group (CSG)	
Data Generation	Full Buffer Traffic	
Path Loss	3GPP Dual Stripe Model 45 dB Minimum Coupling Loss	
Wall Loss	Internal Walls	5 dB attenuation
	External Walls	10 dB attenuation
Shadowing Std. Deviation	Serving Cell	6 dB
	Other Cells	8 dB
Fast Fading	WINNER II CDL Model Indoor Office (A1) - 3 Km/h	
Antenna Configuration	Uniform Linear Array (ULA) 4 antenna elements (0.5λ spacing)	
Scenario B - Indoor Hotspot		
Access Mode	Open Subscriber Group (OSG)	
Data Generation	Full Buffer Traffic	
Path Loss	WINNER II Indoor Hotspot (B3) Model 70 dB Minimum Coupling Loss	
Shadowing Std. Deviation	Line of Sight	3 dB
	Non Line of Sight	4 dB
Fast Fading	WINNER II CDL Model Indoor Hotspot (B3) - 3 Km/h	
Antenna Configuration	Uniform Linear Array (ULA) 4 antenna elements (0.5λ spacing)	

of each of them, summing up 40 APs. In this scenario, the user may connect to any of the available APs, i.e. the network operates in Open Subscriber Group (OSG) access mode. One UE is randomly placed in each square area and each UE selects which AP to connect to based on the highest received power. In case an AP does not serve any UE, it is switched off. In this scenario, pathloss and shadowing are calculated according to the WINNER II Indoor Hotspot (B3) channel model [14].

Small scale fading samples used in the simulation were computed using the WINNER II channel model (Indoor Office (A1) for Scenario A and the Indoor Hotspot (B3) for Scenario B) [14]. We assume uniform linear antenna arrays with four elements separated by $\lambda/2$ in both APs and UEs. In both scenarios, we assume 3 Km/h mobility that may be due to device mobility or other objects moving in the same area causing the channel to change. Table II presents further details on the simulation scenarios.

C. Simulation Results

The network downlink performance was evaluated using a quasi-static system level simulator. The statistical reliability of the simulations is ensured by collecting results from 500

(a) Scenario A - Indoor Office
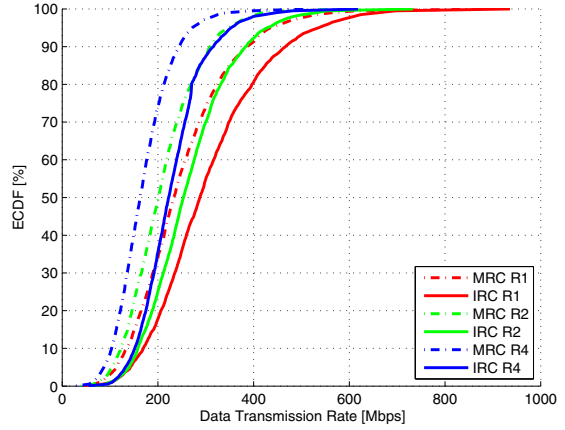
(b) Scenario B - Indoor Hotspot

Fig. 2.   ECDFs showing the data transmission rates in Mbps for both detector types (MMSE-MRC and MMSE-IRC) and different frequency reuse schemes.

<table>
<tr><td colspan="4" align="center">TABLE III
DATA RATES - SCENARIO A [MBPS]</td></tr>
<tr><td>Outage</td><td>MMSE-MRC</td><td>MMSE-IRC</td><td><i>Gains</i></td></tr>
<tr><td>R1</td><td>91.8</td><td>337.4</td><td>(+267.5%)</td></tr>
<tr><td>R2</td><td>314.7</td><td>573.6</td><td>(+82.2%)</td></tr>
<tr><td>R4</td><td>543.4</td><td>697.1</td><td>(+28.3%)</td></tr>
<tr><td>Median</td><td>MMSE-MRC</td><td>MMSE-IRC</td><td><i>Gains</i></td></tr>
<tr><td>R1</td><td>837.5</td><td>1261.2</td><td>(+50.6%)</td></tr>
<tr><td>R2</td><td>1178.4</td><td>1402.4</td><td>(+19.0%)</td></tr>
<tr><td>R4</td><td>1026.0</td><td>1029.6</td><td>(+0.3%)</td></tr>
<tr><td>Peak</td><td>MMSE-MRC</td><td>MMSE-IRC</td><td><i>Gains</i></td></tr>
<tr><td>R1</td><td>2576.7</td><td>2804.2</td><td>(+8.8%)</td></tr>
<tr><td>R2</td><td>2058.3</td><td>2065.1</td><td>(+0.3%)</td></tr>
<tr><td>R4</td><td>1080.0</td><td>1080.0</td><td>-</td></tr>
</table>

<table>
<tr><td colspan="4" align="center">TABLE IV
DATA RATES - SCENARIO B [MBPS]</td></tr>
<tr><td>Outage</td><td>MMSE-MRC</td><td>MMSE-IRC</td><td><i>Gains</i></td></tr>
<tr><td>R1</td><td>113.7</td><td>142.1</td><td>(+25.0%)</td></tr>
<tr><td>R2</td><td>104.7</td><td>139.8</td><td>(+33.5%)</td></tr>
<tr><td>R4</td><td>87.4</td><td>131.9</td><td>(+51.0%)</td></tr>
<tr><td>Median</td><td>MMSE-MRC</td><td>MMSE-IRC</td><td><i>Gains</i></td></tr>
<tr><td>R1</td><td>233.1</td><td>287.9</td><td>(+23.5%)</td></tr>
<tr><td>R2</td><td>201.7</td><td>253.3</td><td>(+25.6%)</td></tr>
<tr><td>R4</td><td>162.8</td><td>222.4</td><td>(+36.6%)</td></tr>
<tr><td>Peak</td><td>MMSE-MRC</td><td>MMSE-IRC</td><td><i>Gains</i></td></tr>
<tr><td>R1</td><td>435.4</td><td>536.6</td><td>(+23.3%)</td></tr>
<tr><td>R2</td><td>346.3</td><td>428.0</td><td>(+23.6%)</td></tr>
<tr><td>R4</td><td>272.3</td><td>353.3</td><td>(+29.8%)</td></tr>
</table>

snapshots. Each snapshot evaluates a time span of 50 frames in which the fast fading channel values are updated every frame, but pathloss and shadowing remain constant. An Empirical Cumulative Distribution Function (ECDF) is then calculated using the throughput of all cells in all snapshots. Three key performance indicators (KPIs) were extracted from the ECDFs, namely peak (95%-tile), median (50%-tile) and outage (5%-tile) data rates.

In both network scenarios, we simulate different frequency reuse schemes by splitting the total bandwidth and assigning only part of the Physical Resource Blocks (PRBs) to each cell. We simulate the scenarios with Reuse 1 (R1), Reuse 2 (R2) and Reuse 4 (R4). In the case of R1, all PRBs are used by all cells, but in the case of R2 and R4, each cell will use only a half and a quarter of all PRBs, respectively. In these two cases, the frequency allocation follows a geometrical pattern that maximizes the distance between two cells using the same set of PRBs.

IV. PERFORMANCE EVALUATION

In this section, we present the numerical simulation results using different combinations of receiver type and planned frequency reuse schemes. First, we discuss the results for Scenario A. Figure 2(a) displays the network throughput performance assuming MMSE-MRC and MMSE-IRC detectors, for different frequency reuse patterns, while Table III presents the KPIs and the relative gains of MMSE-IRC over MMSE-MRC for all Scenario A simulation cases. The MMSE-IRC detector shows considerable gain in terms of outage data rate with respect to MMSE-MRC when R1 is adopted. Such improvement diminishes with higher reuse factors, due to the lower total interference to be rejected. However, the relative data rate gains that MMSE-IRC provides over MMSE-MRC are very large, with improvements of 267.5%, 82.2% and 28.3% in R1, R2 and R4 cases, respectively.

The large data rate gain of MMSE-IRC in scenario A is due to its capability of rejecting the strongest interfering signals.

The particular setup with multiple walls and CSG access mode (i.e., the signal from the serving AP may be weaker than the interferer signals) reduces the overall interference power at the UE and let the most significant interference components be suppressed.

The results also suggest that the negative effects due to multi-stream inter-cell interference on the performance of MMSE-IRC are limited. IRC provides significant outage data rate improvement despite the fact that many cells consistently use spatial multiplexing to transmit multiple data stream to reach higher data rates in this scenario.

Figure 2(b) shows the performance results of both detectors for Scenario B, which represents a different interference situation. As the results in Table IV show, the use of MMSE-IRC improves the outage data rates by 25.0%, 33.5% and 51.0% for the R1, R2 and R4 cases, respectively. Notice that the outage data rate gains actually improve as higher reuse factors are used. In this scenario, the OSG access mode reduces the probability of very strong interference, but on the other hand there are no walls to attenuate the interference generated by the multiple cells that transmit in the same hall. These conditions lead to a situation in which the interference is actually spatially whiter than in Scenario A. As the reuse factor increases, the number of interferers is reduced and the interference becomes less white, i.e. the received signal is dominated by a few strong interferers, and this is the situation in which interference rejection works better.

Furthermore, all cells experience considerable throughput gains, as opposed to Scenario A where the cells in the worst conditions (i.e., lower part of the ECDF) benefit much more than the others. The median data rates are improved by 23.5%, 25.6% and 36.6% and the peak data rates are improved by 23.3%, 23.6% and 29.8% for R1, R2 and R4 cases, respectively. In this scenario, the cells in the top half of the ECDF also experience high interference levels, limiting the throughput to about half of the maximum link capacity. MMSE-IRC rejects more interference in this situation than in the case of the cells in the top half of the ECDFs in Scenario A. However, the median and peak data rate gains are actually reduced as higher reuse factor schemes are used and the overall interference level is reduced.

The results also show that, if higher reuse factors are used in an attempt to reduce the interference levels in Scenario B, the throughputs are actually reduced, because the improvement in SINR is not sufficient to compensate for the reduction in the available bandwidth per cell. Thus, a technique that is capable of reducing the interference levels without limiting the bandwidth is particularly interesting in this scenario.

V. CONCLUSION AND FUTURE WORKS

In this paper, we discussed the potential benefits of IRC as a baseline detector for Beyond 4G small cell networks, where inter-cell interference is identified as the main limiting factor for the throughput performance. Performance results in indoor office and indoor hotspot scenarios have shown the effectiveness of the MMSE-IRC receiver in improving the network throughput with respect to baseline MMSE-MRC detector. The gains are observed even when frequency reuse is used to combat the high interference levels, suggesting that both techniques may be used together to improve the network performance. Also, MIMO rank coordination among neighbour cells does not seem to be required to reach very good results, although it may provide additional gains over those presented in this paper.

The results confirm that the benefits of IRC are large enough to substantiate further studies that will evaluate its performance in situations that are closer to reality, including the effects of channel and interference covariance matrix estimation errors and limitations. Further studies will also address the design of a B4G frame structure that provides the support for IRC to perform consistently, including the adequate design of reference symbols and the necessary means to stabilize the interference during the transmission of a frame.

REFERENCES

[1] P. Mogensen, K. Pajukoski, B. Raaf, E. Tiirola, E. Lähetkangas, I. Z. Kovács, G. Berardinelli, L. G. U. Garcia, L. Hu, and A. F. Cattoni, "B4G local area: high level requirements and system design," Dec. 2012, presented at the *2012 IEEE Global Telecommunications Conference (GLOBECOM 2012)*.

[2] G. Boudreau, J. Panicker, N. Guo, R. Chang, N. Wang, and S. Vrzic, "Interference coordination and cancellation for 4G networks," *Communications Magazine, IEEE*, vol. 47, no. 4, pp. 74–81, Apr. 2009.

[3] V. Chandrasekhar, J. Andrews, and A. Gatherer, "Femtocell networks: a survey," *Communications Magazine, IEEE*, vol. 46, no. 9, pp. 59–67, Sep. 2008.

[4] M. Lampinen, F. Del Carpio, T. Kuosmanen, T. Koivisto, and M. Enescu, "System-level modeling and evaluation of interference suppression receivers in LTE system," in *Vehicular Technology Conference (VTC Spring), 2012 IEEE 75th*, May 2012, pp. 1–5.

[5] K. Pietikainen, F. Del Carpio, H. Maattanen, M. Lampinen, T. Koivisto, and M. Enescu, "System-level performance of interference suppression receivers in LTE system," in *Vehicular Technology Conference (VTC Spring), 2012 IEEE 75th*, May 2012, pp. 1–5.

[6] Y. Ohwatari, N. Miki, T. Abe, and H. Taoka, "Investigation on advanced receiver employing interference rejection combining in asynchronous network for LTE-Advanced downlink," in *Vehicular Technology Conference (VTC Spring), 2012 IEEE 75th*, May 2012, pp. 1–6.

[7] Y. Sano, Y. Ohwatari, N. Miki, A. Morimoto, and Y. Okumura, "Investigation on link performance modeling of advanced receiver employing interference rejection combining in system level evaluation for LTE-Advanced downlink," in *2012 International Symposium on Wireless Communication Systems (ISWCS)*, Aug. 2012, pp. 919–923.

[8] S. Haykin, M. Sellathurai, Y. de Jong, and T. Willink, "Turbo-MIMO for wireless communications," *Communications Magazine, IEEE*, vol. 42, no. 10, pp. 48–53, Oct. 2004.

[9] J. Winters, "Optimum combining in digital mobile radio with cochannel interference," *Selected Areas in Communications, IEEE Journal on*, vol. 2, no. 4, pp. 528–539, Jul. 1984.

[10] "Enhanced performance requirement for LTE User Equipment (UE)," 3GPP, TR 36.829 v11.1.0, Jan. 2013. [Online]. Available: http://www.3gpp.org

[11] J. Choi, *Optimal Combining and Detection: Statistical Signal Processing for Communications*. Cambridge: Cambridge University Press, 2010.

[12] "Evolved Universal Terrestrial Radio Access (E-UTRA); Physical channels and modulation," 3GPP, TS 36.211 v11.1.0, Dec. 2012. [Online]. Available: http://www.3gpp.org

[13] "Evolved Universal Terrestrial Radio Access (E-UTRA); Further advancements for E-UTRA physical layer aspects," 3GPP, TR 36.814 v9.0.0, Mar. 2010. [Online]. Available: http://www.3gpp.org

[14] P. Kyösti et al, "WINNER II Channel Models," IST-WINNER, D1.1.2 v1.1, Sep. 2007. [Online]. Available: https://www.ist-winner.org/WINNER2-Deliverables/D1.1.2v1.1.pdf